Solid-State ^{13}C NMR Analyses of the Microphase-Separated Structure of Polyurethane Elastomer

Masato Ishida* and Kunio Yoshinaga

Takeda Chemical Industries, Yodogawa, Osaka 532, Japan

Fumitaka Horii*

Institute for Chemical Research, Kyoto University, Uji, Kyoto 611, Japan

Received January 16, 1996; Revised Manuscript Received September 19, 1996[⊗]

ABSTRACT: Solid-state ^{13}C NMR analyses have been performed to obtain information about the microphase-separated structure for polyurethane (PUR) elastomer, which is prepared from *p*-phenylene diisocyanate (PPDI), poly(tetramethylene oxide) (PTMO), and 1,4-butanediol (BD). ^{13}C spin−lattice relaxation time (T_{1C}) analyses have revealed that three components with different T_{1C} values exist for the PPDI and BD residues, while two components are observed for the PTMO carbons. The longest T_{1C} components of the PPDI and BD carbons are assigned to the crystalline component, whereas the PTMO carbons with shorter T_{1C}'s and the PPDI and BD residues with shortest T_{1C}'s are ascribed to the rubbery component. Moreover, the PPDI and BD residues with the medium T_{1C} values and the PTMO carbons with the longer T_{1C} values are found to be assignable to the interfacial component by the T_{1C} measurement for the component selectively created through the ^1H spin diffusion from the rubbery component. The mass fraction values of the three components thus assigned are determined for the respective structural units; in the PPDI units, for example, the mass fraction values 0.40 for the crystalline component, 0.16 for the interfacial component, and 0.44 for the rubbery amorphous component. On the basis of these results, the microphase-separated structure is discussed for the PUR elastomer.

Introduction

It is well-known that polyurethane (PUR), which is a type of block copolymer with hard and soft segments, has a microphase-separated structure mainly composed of the crystalline and rubbery regions. Since the structure should be associated with macroscopic PUR properties, many studies of the structure have been performed by using various analytical methods, such as small-angle X-ray scattering (SAXS),[1−6] differential scanning calorimetry (DSC),[4,6,7] transmission electron microscoyp (TEM),[2,8] dynamic mechanical analysis,[3] Raman spectroscopy,[8] and solid-state NMR spectroscopy.[9,10] For example, SAXS revealed the reversible or irreversible change in the microphase-separated structure with temperature for PUR samples with different molar ratios of the soft segment and chain extender.[1] The similar structural change induced by postannealing was also examined by this method.[4] DSC also provides important information about the extent of the microphase separation by monitoring glass transition processes and the melting endotherms in detail.[4,7] However, more detailed information of the distribution of hard and soft segments in the crystalline and noncrystalline phases has not yet been provided by those previous structural studies.

High-resolution solid-state ^{13}C NMR spectroscopy is very powerful in characterizing the detailed structure and molecular motion of solid polymers[11] including polyurethanes.[9,10] In particular, we have clarified the phase structure composed of the crystalline, crystalline−amorphous interfacial, and amorphous regions for different crystalline polymers[12−17] by analyzing ^{13}C resonance line shapes, spin−lattice relaxation, and spin−spin relaxation behaviors, ^1H spin diffusion processes, and so on. The characteristic crystalline−noncrystalline structure and hydrogen bonding have been also revealed for native cellulose[18,19] and poly(vinyl alcohol)[20,21] by the similar ^{13}C NMR analysis.

In this work, we have examined the microphase-separated structure by using similar ^{13}C NMR analysis previously employed, particularly focusing our attention on the characterization of the distribution of each segment into the crystalline, interfacial, and rubbery regions.

Experimental Section

Sample. The polyurethane sample used in this study was prepared by using the following two-step method. The soft segment oligomer, poly(tetramethylene oxide) (PTMO), with a number-average molecular weight of 1000, was dehydrated by heating at 100 °C for 2 h with stirring under vacuum. The $\bar{M}_w/\bar{M}_n$ ratio for the PTMO measured by gel-permeation chromatography (GPC) was 1.57. Then a given amount of *p*-phenylene diisocyanate (PPDI) (NCO/OH molar ratio = 2.0) was added to the dehydrated PTMO at once. This mixture was reacted for 2 h with stirring under nitrogen. The reaction time is so long that there is no terminal OH groups. Next, 1,4-butanediol (BD) chain extender (OH/NCO molar ratio = 0.98), which was preheated to 100 °C, was mixed with the prepolymer rapidly within 30 s, and then the mixture was poured into a mold with a cavity of dimensions 120 × 315 × 2 mm^3. The mold was transferred to an oven and reacted at 110 °C for 20 h.

At the end of the first step, the mole fraction of the unreacted PPDI was 0.144 mol %, which was determined by GPC. If the reaction rate of the isocyanate group in the diisocyanate (PPDI entirely unreacted) with PTMO is the same as that in the monoisocyanate (PPDI reacted with PTMO at one side such as *PPDI*−PTMO−PPDI), the mole fraction of the unreacted PPDI should be 0.25 at the end of the first step. This value was derived from Flory's equation[22] for the complete reaction in the one-component exceeded system; $P_x = r^{x/2}(1 - r)r^{-1/2}$, where P_x is the mole fraction of *x*-mer and r ($r < 1$) is the mole ratio of PPDI and PTMO. Since the calculated value is smaller than 0.144, the reaction rate of the diisocyanate must be higher than that of the monoisocyanate. We estimated the ratio of the rate constants for the diisocyanate (r_1) and the monoisocyanate (r_2) using the simple statistical

[⊗] Abstract published in *Advance ACS Abstracts,* December 1, 1996.

S0024-9297(96)00053-8 CCC: $12.00

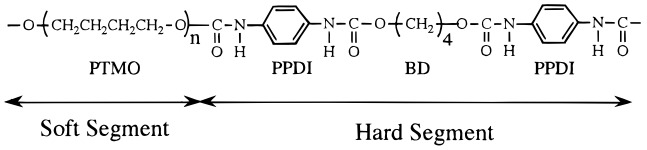

Figure 1. The structural units of polyurethane elastomer used in this work.

calculation by a computer, in which all possible reactions were considered. As a result, r_1/r_2 was determined to be 10.5, which is close to the value previously reported for the reactions of PPDI with 1-butanol.[23] Using the ratio, we assumed possible structural entities at the end of the first step as follows: PPDI (0.146), PPDI−PTMO−PPDI (0.729), PPDI−PTMO−PPDI−PTMO−PPDI (0.106), PPDI−PTMO−PPDI−PTMO−PPDI−PTMO−PPDI (0.0154), and so on, where the values in parentheses are their mole fractions. On the basis of these results, the mole fractions for the hard segments consisting of PPDI and BD residues, which were obtained at the second step of the reaction with BD, were calculated as follows: −PPDI−BD−PPDI− (0.85), −PPDI−BD−PPDI−BD−PPDI− (0.13), −PPDI−BD−PPDI−BD−PPDI−BD−PPDI− (0.02), and so on. Here, it was assumed that the free PPDI had the same reactivity with BD as the prepolymer. The validity of this assumption will be elucidated later on the basis of the results obtained in this work.

Figure 1 shows the main structural unit produced by the reaction of the prepolymer PPDI−PTMO−PPDI with BD, where PPDI and BD belong to the hard segment and PTMO to the soft segment. The glass transition and melting temperatures of this sample were determined as −43 and 170 °C by DSC, respectively. In order to prevent a possible change of structure during NMR measurements, the sample was annealed at 170 °C for 1 h under an atmosphere of nitrogen.

^{13}C NMR Measurements. Solid-state ^{13}C NMR measurements were performed on a JEOL JNM-EX270 spectrometer equipped with a variable temperature MAS system operating at 67.8 MHz under a static magnetic field of 6.35 T. The sample, a cutoff portion about 1 mm in diameter, was packed in a 6 mm diameter zirconia rotor. The pulse recycle time was 5 s. The number of scans was about 1000, but it was increased up to about 3000 in the ^1H spin diffusion experiment; the ^1H 90° pulse width was 4.0 μs and the contact time for the cross polarization (CP) process was 2.0 ms throughout this work. The magic angle spinning (MAS) rate was set to 5 kHz to avoid the overlapping of spinning side bands on other resonance lines. ^{13}C chemical shifts were expressed as values relative to tetramethylsilane (Me_4Si) by using the CH_3 line at 17.36 ppm of hexamethylbenzene crystals as an external reference.

Results and Discussion

CP/MAS ^{13}C NMR Spectrum. Figure 2 shows 67.8 MHz CP/MAS ^{13}C NMR spectrum of the PUR sample measured at 30 °C. The assignment of each resonance line has been made on the basis of the results for the solution-state spectrum[24] as well as the quaternary carbon-enhanced spectrum obtained by dipolar diphasing method.[25] The upfield shoulder (C3U) at about 120 ppm can be assigned to the rubbery component of the C3 carbon, because the ^{13}C spin−lattice relaxation time (T_{1C}) of this line is as short as 0.37 s, as shown later in detail. Since the respective resonance lines assignable to the hard and soft segments are separately observed, the microphase-separated structure and molecular motion will be able to be analyzed by considering the contributions from these segments.

^1H Spin−Lattice Relaxation Times (T_{1H}, $T_{1\rho H}$) in the Laboratory Frame and in the Rotating Frame. In order to estimate the domain size of the microphase-separated structure, T_{1H} and $T_{1\rho H}$ values were measured at 30 °C by the pulse sequence equipped in the JEOL spectometer. Table 1 lists their values for the respective

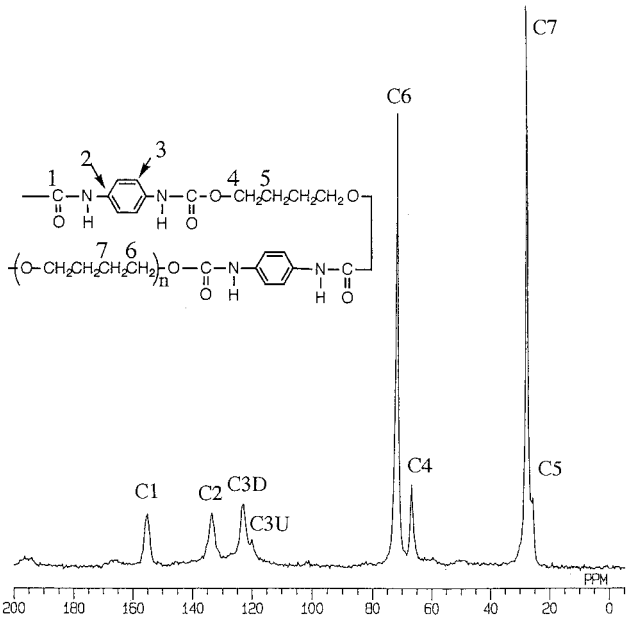

Figure 2. 67.8 MHz CP/MAS ^{13}C NMR spectrum of PUR at 30 °C.

Table 1. T_{1H}, $T_{1\rho H}$, and T_{2H} Values of the Respective Carbons of PUR Measured at 30 °C

	hard segment					soft segment	
	C1	C2	C3D[a]	C3U[a]	C4	C5	C6
T_{1H}/ms	430	439	433	*b*	422	424	434
$T_{1\rho H}$/ms	9.4	9.0	9.2	*b*	9.0	11.4	11.6
T_{2H}/μs	8	8	7	25	8	55	48

[a] C3D and C3U indicate the downfield and upfield resonance lines for the C3 carbon, respectively. [b] Not measured.

carbons. All T_{1H} values are almost the same, indicating that the ^1H spins in the different domains are fully exchanged during the time corresponding to T_{1H}. Therefore, the domain size of the microphase-separated structure can be roughly estimated as less than 20 nm by simply using the one-dimensional diffusion equation[26] as follows:

$$\langle x^2 \rangle^{1/2} = (4/3)Dt \qquad (1)$$

where x is the distance and t is the time for spin diffusion. D is the diffusion coefficient, which is here assumed to be 5×10^{-12} cm^2/s.[26] On the other hand, there is a significant difference in $T_{1\rho H}$ between the hard and soft segments, probably as a result of the insufficient average of ^1H spins in a time scale of $T_{1\rho H}$. This fact suggests also through the use of eq 1 that the domain size will be at least a few nanometers in this sample.

^{13}C Spin−Lattice Relaxation Times. In order to correlate each structural unit to the microphase-separated structure, ^{13}C spin-lattice relaxation behavior has been measured at 30 °C for the respective resonance lines by CPT1 pulse sequence.[27] In Figure 3 the logarithmic peak intensity of the C2 carbon is plotted against the decay time t. Since the decay curve does not appear to be a single exponential, it is analyzed in terms of a few components with different T_{1C} values by the least-squares method. The solid line is the result calculated by assuming three components with different T_{1C}'s, where the exponential decay of each component is also shown as broken line. The experimental points agree well with the calculated curve, indicating that the

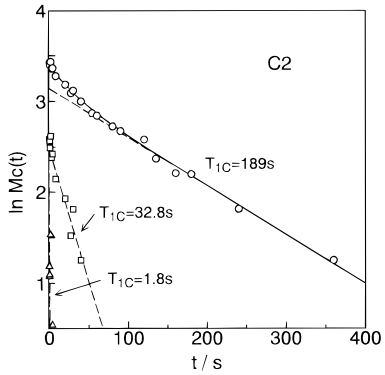

Figure 3. Semilogarithmic plots of peak intensities ($M_C(t)$) for the C2 resonance line as a function of time.

Table 2. T_{1C} Values of the Respective Carbons of PUR Measured at 30 °C

T_{1C}/s							
hard segment						soft segment	
C1	C2	C3D	C3U	C4	C5	C6	C7
172	187	145	*a*	126	121	*a*	*a*
26.6	34.4	21.6	*a*	8.8	7.9	7.4	4.4
3.4	1.6	*a*	0.37	0.48	0.37	0.35	0.34

[a] Not detected.

C2 resonance line contains three components with different T_{1C} values. Similar two or three components are found to exist for other resonance lines.

Table 2 gives T_{1C} values of the respective resonance lines of the PUR sample thus obtained. Interestingly, the PPDI and BD carbons have three T_{1C} values, while only two T_{1C}'s appear for the PTMO carbons. The component with the longest T_{1C} values for the PPDI and BD carbons should be assigned to the crystalline component, because the existence of the crystalline component is clearly confirmed by the X-ray diffraction and DSC methods. On the other hand, the component with T_{1C}'s of less than 1 s for the PTMO carbons will be assigned to the rubbery component, because the T_{1C} measurement was carried out at 30 °C, which is well-above the glass transition temperature (−43 °C) of the poly(tetramethylethylene oxide). Judging from the level of T_{1C} values, the component with the shortest T_{1C} values for the PPDI and BD carbons should be also ascribed to the rubbery component. This indicates that the hard segment is also found in the noncrystalline region with rubberlike mobility. In contrast, it seems somewhat difficult to make an assignment for the component with medium T_{1C}'s for the PPDI and BD carbons and for the component with longer T_{1C}'s for the PTMO carbons. In the previous report,[28] those components were simply assigned to the interfacial component, which is defined as a component located in between the crystalline and rubbery amorphous regions. However, this assignment should be reconfirmed by the following T_{1C} measurements combined with a ^{1}H spin diffusion measurement.

Characterization of the Interfacial Component. Figure 4 shows the pulse sequence used for the characterization of the component with the medium T_{1C} value recognized for the downfield line (C3D) of the C3 carbon. The pulse sequence, which is prepared by the combination of the Goldman−Shen pulse sequence,[29] CP technique, and inversion recovery method, is composed of five periods. The first is the preparation period (τ_t), in which the ^{1}H magnetization gradient is created using

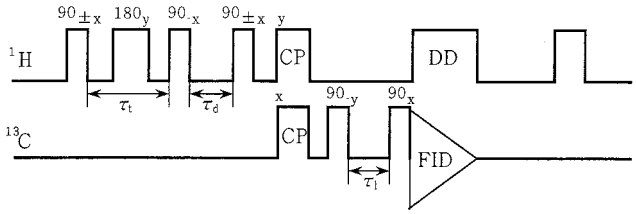

Figure 4. Pulse sequence combined with the Goldman−Shen pulse sequence, the cross polarization technique, and the inversion recovery method.

the difference in ^{1}H spin−spin relaxation times (T_{2H}) of the respective components. At the end of this period only the magnetization of the rubbery component is left. The second is the diffusion period (τ_d), during which ^{1}H spins diffuse from the rubbery component to other components. At the later stage of this period the effect of the T_{1H} relaxation appears, although such an effect may be suppressed for a shorter τ_d in the pulse sequence. The third is the CP period, in which the ^{1}H magnetization existing at the end of the diffusion period is transferred into the ^{13}C magnetization. The fourth is the ^{13}C spin−lattice relaxation period (τ_l), in which the ^{13}C magnetization produced in the CP period (period 3) is flipped to the $-z$ axis and is relaxed to the equilibrium state. The fifth is the detection period. In actual measurements the spin temperature alternation method was employed in the CP process. This pulse sequence will be effectively used to determine the T_{1C} value for the component closely located to the rubbery component.

First we have examined the effectiveness of the Goldman−Shen pulse sequence as well as the ^{1}H spin diffusion process by using the pulse sequence without the ^{13}C spin−lattice relaxation period (period 4) shown in Figure 4. Figure 5 shows one example of the results in which the τ_t value was set to 40 μs. The resonance lines for the C3U, C6, and C7 carbons are exclusively observed at τ_d = 0.1 ms as a result of the longer T_{2H} values of these carbons (cf. T_{2H} values for the respecitve carbons in Table 1). However, the C1, C2, C3D, C4, and C5 lines remarkably increase in intensity with increasing τ_d value. Since the T_{1H} effect is suppressed for a short τ_d in the pulse sequence used here, the increase in intensity is really due to the ^{1}H spin diffusion from the rubbery region to the neighboring region containing these carbons.

Next we have measured T_{1C} values for the components newly observed as a result of the ^{1}H spin diffusion from the rubbery region. Figure 6 shows partially relaxed ^{13}C NMR spectra for the C1, C2, C3D, and C3U carbons obtained at τ_t = 40 μs and τ_d = 7 ms by the pulse sequence shown in Figure 4. The C3U line seems to recover to the thermal equilibrium state at τ = 2 s, while the C3D line is still increasing in intensity around τ_t = 280 s.

In Figure 7 is plotted the peak intensity of the C3D line shown in Figure 6 against the time τ_l. The solid line is the result calculated by assuming that two components may contribute to the ^{13}C spin-relaxation recovery process as described as follows:

$$M_C(\tau_l) = M_{\alpha\infty} + (M_\alpha - M_{\alpha\infty})\exp(-\tau_l/T_{1C\alpha}) + M_{\beta\infty} + (M_\beta - M_{\beta\infty})\exp(-\tau_l/T_{1C\beta}) \quad (2)$$

Here, $T_{1C\alpha}$ and $T_{1C\beta}$ are the ^{13}C spin−lattice relaxation times of components α and β. M_j and $M_{j\infty}$ (j = α or β)

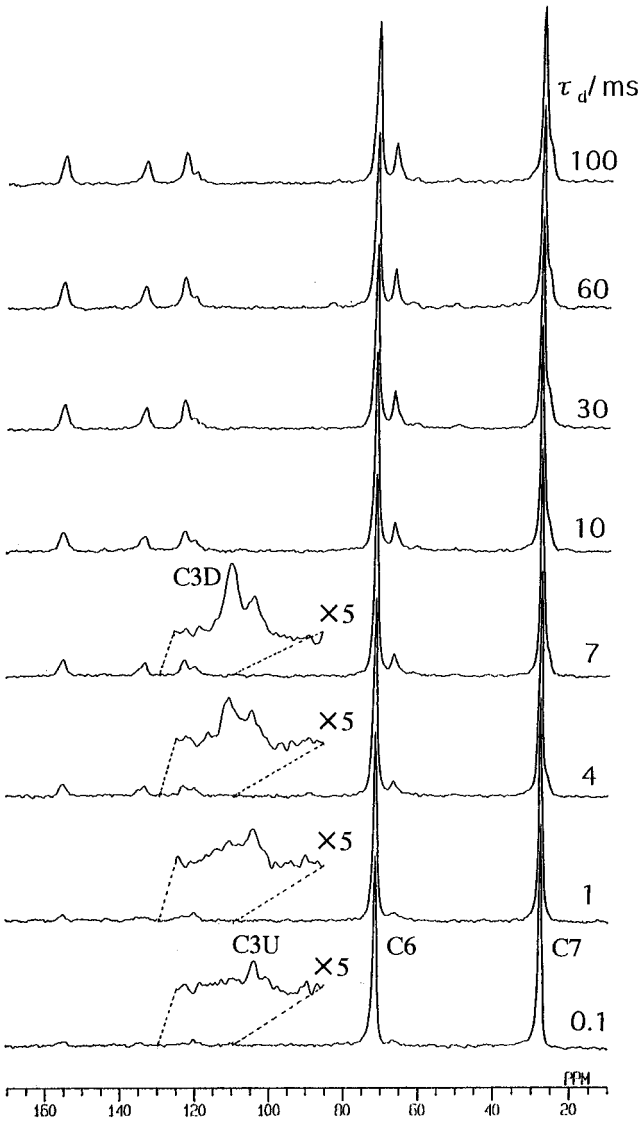

Figure 5. ^{1}H spin diffusion measurement from the rubbery region (C3D, C6, C7) to other regions (C3U, etc.) in PUR at 30 °C with $\tau_t = 80\ \mu s$ for the pulse sequence shown in Figure 4.

Table 3. Optimal Parameters Used for the Analysis of the C3D Resonance Line Shown in Figure 7 in Terms of Eq 2

component α			component β		
$T_{1C\alpha}$	M_α	$M_{\alpha\infty}$	$T_{1C\beta}$	M_β	$M_{\beta\infty}$
23	−1.67	1.40	140	0.028	3.55

are the magnetizations of the corresponding components at $\tau_l = 0$ and $\tau_l = \infty$, respectively. The experimental data indicated as open circles are in good accord with the calculated result which is optimized by a computer least-squares method. Here, the respective components are indicated as broken lines in Figure 7. All parameters used for the optimal fitting are shown in Table 3. As can be seen in this table, the T_{1C} values of components α and β are respectively 23 and 140 s, which are in good accord with the values shown for the C3 carbon in Table 2. Moreover, the initial magnetization M_α of the component α is −1.67, whereas the corresponding value M_β is almost zero for component β. This indicates that component α with $T_{1C} = 23$ s is the component observed as a result of the ^{1}H spin diffusion from the rubbery region. It is, therefore, concluded that the component with $T_{1C} = 23$ s, which corresponds to T_{1C} = 21.6 s for the C3D carbon in Table 2, should be assigned to the component directly connecting to the rubbery component, that is, the interfacial component.

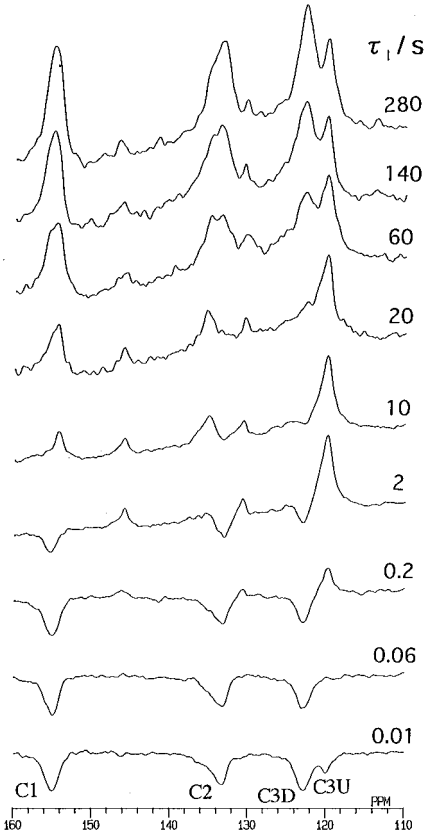

Figure 6. Inversion recovery measurement for the components produced by the ^{1}H spin diffusion from the rubbery component at 30 °C with $\tau_t = 80\ \mu s$ and $\tau_d = 7$ ms for the pulse sequence shown in Figure 4.

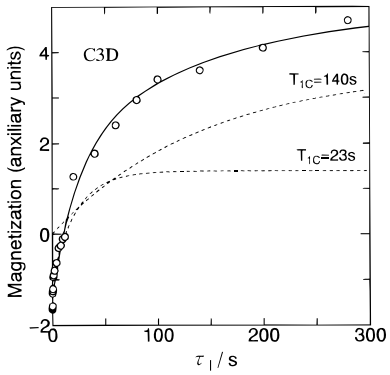

Figure 7. Plots for the peak intensity of the C3D resonance line shown in Figure 6 as a function of time τ_l. The solid line is the composite curve of the two components with different T_{1C} values indicated as broken lines.

Figure 8 shows the dipolar-decoupling (DD)/MAS ^{13}C NMR spectrum of the PUR samples measured at room temperature by a 45° single pulse sequence. This spectrum quantitatively reproduces the contributions from all structural components, since the pulse repetition time for the 45° single pulse sequence was set to 600 s, which is longer than 3 times the longest T_{1C} value shown in Table 2. In contrast with the CP/MAS spectrum shown in Figure 2, the upfield component of the C3 line (C3U) is clearly observed due to the increase of the intensity of this line. Figure 8 also shows the result of the computer line shape analysis for the C3D and C3U resonance lines. Here, each line was assumed

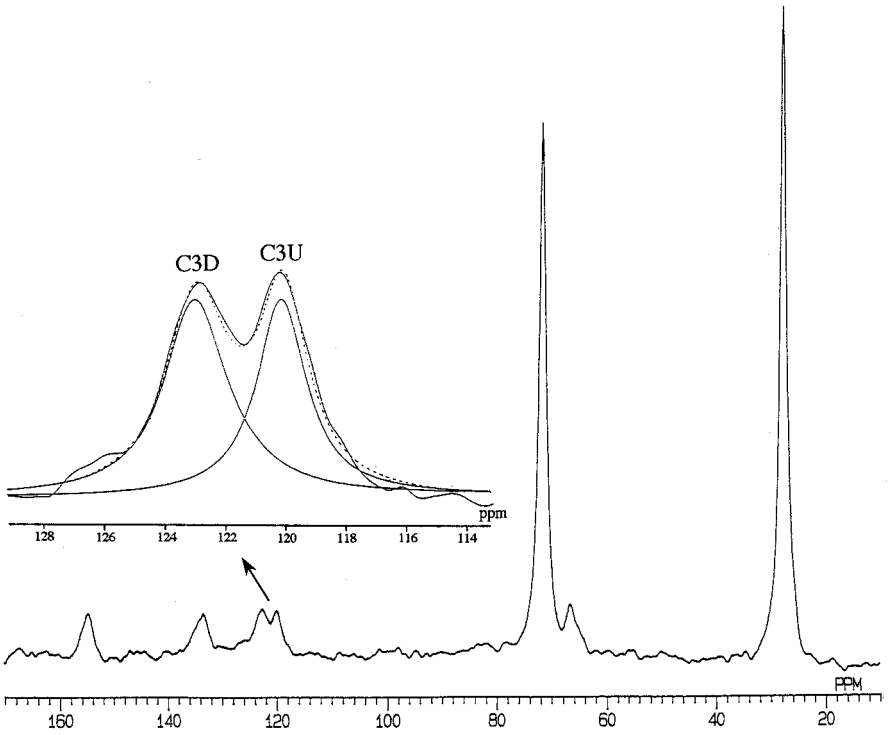

Figure 8. DD/MAS ^{13}C NMR spectrum of PUR measured at 30 °C by the 45° single pulse sequence with the repetition time of 600 s.

Table 4. Mole Fractions of the Crystalline, Interfacial, and Rubbery Components for the Respective Structural Units[a]

	PPDI	BD	PTMO
crystalline	0.40 (0.20)	0.52 (0.13)	0 (0)
interfacial	0.16 (0.08)	0.17 (0.04)	0.04 (0.01)
rubbery	0.44 (0.22)	0.31 (0.08)	0.96 (0.24)

[a] The values in parentheses are the mole fractions of the respective components for the all structural units.

to be described as Lorentzian. The composite curve for each line, which is shown by a broken line, is in good agreement with the experimental spectrum. The integrated fractions of the C3D and C3U lines obtained by this analysis are 0.56 and 0.44, respectively. On the other hand, the fractions of the crystalline and interfacial components, which are involved in the C3D line, are 0.72 and 0.28, respectively, as estimated for the $M_{\alpha\infty}$ and $M_{\beta\infty}$ values in Table 3. Accordingly, the mole fractions of the respective components can be estimated for the C3 carbon in the PPDI residue as follows: 0.40, 0.16, and 0.44 for the crystalline, interfacial, and rubbery amorphous components.

Table 4 lists the mole fractions of the crystalline, interfacial, and rubbery components for the respective structural units of the PUR sample. The fractions for the BD unit were determined by the T_{1C} measurement using the CPT1 pulse sequence, while the fractions for the PTMO unit were estimated by the saturation recovery measurement. The PPDI/BD mole ratio was determined as 1.5 in the crystalline region by using the values in Table 4 and the quantities of the starting materials.

On the basis of these results, a schematic structure model is shown for the PUR sample in Figure 9. Here, we assume that crystallites are composed of the PPDI−BD−PPDI units, their extended length being about 2.5 nm. Most of the PPDI−BD−PPDI−BD−PPDI and PPDI−BD−PPDI−BD−PPDI−BD−PPDI units may be

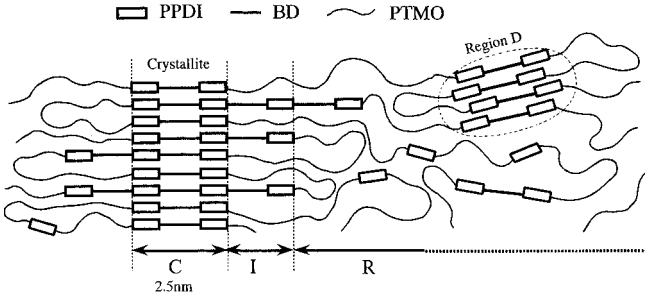

Figure 9. Schematic representation of the microphase-separated structure of the PUR sample used in this work.

included in the crystallites, because they would become nuclei for the crystallization owing to the lower molecular mobility. When the crystallite as shown in Figure 9 is formed, the excessive, protruded BD−PPDI units in those structural units many contribute to the interfacial region. However, there are two problems with this model. One is that the mole ratio of PPDI/BD is as low as 1.5 in the crystalline region, as shown in Table 4. The other is that equal mole fractions of the PPDI and BD units are not fulfilled in the interfacial region, as also seen in Table 4. Therefore, we must additionally introduce a disordered region such as region D (Figure 9), where the PPDI−BD−PPDI units aggregate with each other without three-dimensional ordering. The core part of the region should contribute to the longest T_{1C} component similarly to the crystalline component, whereas the surfacial part may be detected as the interfacial component by CP/MAS ^{13}C NMR. Since the mole fraction of the interfacial component is very low for the PTMO sequence, the probability of region D existing would be rather high compared to that of the crystallites. Any way, there is too great a distribution in the structure of this sample. A more detailed characterization will be carried out in the near future for samples with less distribution, at least with no distribution for the hard segment.

Conclusion

The microphase-separated structure for PUR, which is composed of PPDI, PTMO, and BD, has been elucidated by high-resolution solid-state ^{13}C NMR spectroscopy and the following conclusions have been obtained.

(1) ^{13}C spin−lattice relaxation time (T_{1C}) analyses carried out at room temperature have confirmed that three components with different molecular mobilities exist for the PPDI and BD residues, whereas two components are observed for the PTMO sequence. The PPDI and BD carbons with the longest T_{1C} values can be assigned to the crystalline component, while the PTMO carbons with shorter T_{1C}'s and the PPDI and BD carbons with shortest T_{1C}'s are ascribed to the rubbery component.

(2) The existence of the interfacial region between the crystalline and rubbery regions has been examined by the T_{1C} measurement for the component close to the rubbery component. As a result, the PPDI and BD carbons with medium T_{1C} values and the PTMO carbons with the longer T_{1C} values are assigned to the interfacial component.

(3) The line shape analysis of the DD/MAS ^{13}C NMR spectrum obtained by utilizing the thermal equilibrium magnetization and the T_{1C} analysis have determined the mole fractions of the crystalline, interfacial, and the rubbery components for the respective structural units.

References and Notes

(1) Desper, C. R.; Byrne, C. A.; Li, Y.; Chu, B. *Macromolecules* **1995**, *28*, 4213.
(2) Chen-Tsai, C. H. Y.; Thomas, E. L.; MacKnight, W. J.; Schneider, N. S. *Polymer* **1986**, *27*, 659.
(3) Kohjiya, S.; Yamato, T.; Ikeda, Y.; Yamashita, S.; Saruyama, Y.; Hayashi, H.; Yamamoto, N.; Yamashita, H. *J. Soc. Rheol. Jpn.* **1990**, *18*, 202.
(4) Li, Y.; Gao, T.; Liu, J.; Linliu, K.; Desper, C. R.; Chu, B. *Macromolecules* **1992**, *25*, 7365.
(5) Chu, B.; Gao, T.; Li, Y.; Wang, J.; Desper, C. R.; Byrne, C. A. *Macromolecules* **1992**, *25*, 5274.
(6) Koberstein, J. T.; Russell, T. P. *Macromolecules* **1986**, *19*, 714.
(7) Li, Y.; Ren, Z.; Zhao, M.; Yang, H.; Chu, B. *Macromolecules* **1993**, *26*, 612.
(8) Nitzsche, S. A.; Hsu, S. L.; Hammond, P. T.; Rubner, M. F. *Macromolecules* **1992**, *25*, 2391.
(9) Tao, H.; Rice, D. M.; MacKnight, W. J.; Hsu, S. L. *Macromolecules* **1995**, *28*, 4036.
(10) Okamoto, D. T.; O'Connell, E. M.; Root, T. W. *J. Polym. Sci.: Part B: Polym. Phys.* **1993**, *31*, 1163.
(11) For example, (a) Schmidt-Rohr, K.; Spiess, H. W. *Multidimensional Solid-State NMR and Polymers*; Academic Press: Lonon, 1994. (b) Blumich, B. (Ed.) *NMR Basic Principles and Progress. Solid-State NMR III Organic Matter*.; Springler-Verlag: Berlin, 1994. (c) Tycho, R. (Ed.) *Nuclear Magnetic Resonance Probes of Molecular Dynamics*; Kluwer Academic Publishers: Dordrecht, 1994.
(12) Kitamaru, R.; Horii, F.; Murayama, K. *Macromolecules* **1986**, *19*, 636.
(13) Hirai, A.; Horii, F.; Kitamaru, R.; Fatou, J. G.; Bello, A. *Macromolecules* **1990**, *23*, 2913.
(14) Saito, S.; Moteki, Y.; Nakagawa, M.; Horii, F.; Kitamaru, R. *Macromolecules* **1990**, *23*, 3257.
(15) Kimura, T.; Neki, K.; Tamura, N.; Horii, F.; Nakagawa, M.; Odani, H. *Polymer* **1992**, *23*, 493.
(16) Tsuji, H.; Horii, F.; Nakagawa, M.; Ikada, Y.; Odani, H.; Kitamaru, R. *Macromolecules* **1992**, *25*, 4114.
(17) Kitamaru, R.; Horii, F.; Zhu, Q.; Bassett, D. C.; Olley, R. H. *Polymer* **1994**, *35*, 1171.
(18) Yamamoto, H.; Horii, F. *Macromolecules* **1993**, *26*, 1313.
(19) Yamamoto, H.; Horii, F. *Cellulose* **1994**, *1*, 57.
(20) Horii, F.; Hu, S.; Ito, T.; Odani, H.; Matsuzawa, S.; Yamaura, K. *Polymer* **1992**, *33*, 2299.
(21) Hu, S.; Tsuji, M.; Horii, F. *Polymer* **1994**, *35*, 2516.
(22) Flory, P. J. *J. Am. Chem. Soc.* **1936**, *58*, 1877.
(23) Burkus, J.; Eckert, C. F. *J. Am. Chem. Soc.* **1958**, *80*, 5948.
(24) Delides, C.; Pethrick, R. A.; Cunliffe, A. V.; Klein, P. G. *Polymer* **1981**, *22*, 1205.
(25) Opella, S. J.; Frey, M. H. J. *J. Am. Chem. Soc.* **1979**, *101*, 5854.
(26) Havens, J. R.; VanderHart, D. L. *Macromolecules* **1985**, *18*, 1663.
(27) Torchia, D. A. *J. Magn. Reson.* **1981**, *44*, 117.
(28) Taguchi, K.; Nakagawa, M.; Horii, F.; Odani, H. *Polym. Prepr. Jpn.* **1988**, *37*, 2489.
(29) Goldman, M.; Shen, L. *Phys. Rev.* **1966**, *144*, 321.

MA960053U